



Published in final edited form as:

Nat Biotechnol. 2013 July ; 31(7): 630–637. doi:10.1038/nbt.2620.

Chaperones as thermodynamic sensors of drug–target interactions reveal kinase inhibitor specificities in living cells

Mikko Taipale¹, Irina Krykbaeva¹, Luke Whitesell¹, Sandro Santagata^{1,2}, Jianming Zhang³, Qingsong Liu³, Nathanael S. Gray³, and Susan Lindquist^{1,4,5}

¹Whitehead Institute for Biomedical Research, Cambridge, MA 02142, USA

²Department of Pathology, Brigham and Women's Hospital and Harvard Medical School, Boston, MA 02115, USA

³Biological Chemistry & Molecular Pharmacology, Harvard Medical School and Department of Cancer Biology, Dana-Farber Cancer Institute, Boston, MA 02115, USA

⁴Department of Biology, Massachusetts Institute of Technology, Cambridge, MA 02142, USA

⁵Howard Hughes Medical Institute, Cambridge, MA 02142, USA

The interaction between the HSP90 chaperone and its client kinases is sensitive to the conformational status of the kinase, and stabilization of the kinase fold by small molecules strongly decreases chaperone interaction¹. Here we exploit this observation and assay small-molecule binding to kinases in living cells, using chaperones as 'thermodynamic sensors'. The method allows determination of target specificities of both ATP-competitive and allosteric inhibitors in the kinases' native cellular context in high throughput. We profile target specificities of 30 diverse kinase inhibitors against over 300 kinases. Demonstrating the value of the assay, we identify ETV6-NTRK3 as a target of the FDA-approved drug crizotinib. Crizotinib inhibits proliferation of ETV6-NTRK3-dependent tumor cells with nanomolar potency and induces the regression of established tumor xenografts in mice. Finally, we show that our approach is applicable to other chaperone and target classes by assaying HSP70/steroid hormone receptor and CDC37/kinase interactions, suggesting that chaperone interactions will have broad application in detecting drug-target interactions *in vivo*.

Users may view, print, copy, download and text and data-mine the content in such documents, for the purposes of academic research, subject always to the full Conditions of use: http://www.nature.com/authors/editorial_policies/license.html#terms

Corresponding author: Susan Lindquist, lindquist_admin@wi.mit.edu.

AUTHOR CONTRIBUTIONS

M.T. and S.L. planned the project. M.T. designed the experiments, developed the assay, performed the experiments together with I.K., and analyzed the data. Xenograft experiments were done by L.W., and S.S. performed immunohistochemistry on tumor samples. J.Z. tested BCR-ABL variants for GNF-2 sensitivity in BaF/3 cells. J.Z., Q.L., and N.S.G. synthesized and provided kinase inhibitors and helped design experiments. M.T. and S.L. wrote the paper with input from all co-authors.

COMPETING FINANCIAL INTERESTS

M.T. and S.L. are named inventors on a patent application on the technology described in this manuscript and co-founders of an early-stage startup company utilizing the technology for drug screening.

INTRODUCTION

Determining the specificity of small molecules is important for research scientists, medicinal chemists, clinicians and their patients alike. In the laboratory, small molecule drugs are commonly used as chemical probes, and the meaningful interpretation of the results of such experiments requires detailed knowledge of drug's targets. In the pharmaceutical industry, target profiling can be used to identify candidate targets for compounds discovered in cell-based screens and to guide medicinal chemistry efforts to obtain a favorable target spectrum during lead compound optimization. In the clinic, experimental drugs often show in unexpected efficacy or toxicity that can sometimes be rationalized through more thorough target profiling. Moreover, identification of additional targets of an approved drug with previously established safety profile can facilitate its rapid repurposing to new diseases.

The protein kinase family illustrates the challenges inherent to target profiling. Almost all protein kinases share the same conserved fold, and consequently, developing inhibitors that are both highly potent and highly selective has proven difficult². Given the pharmaceutical interest in drugging protein kinases, several high-throughput methods have been developed for profiling inhibitor specificities *in vitro*^{3–8}. However, the correlation between *in vitro* results and *in vivo* efficacy has often been disappointing^{9, 10}. Chemical proteomic based approaches have shown considerable promise for inhibitor profiling^{11, 12}. However, they are not well suited to profiling allosteric inhibitors, which are not competitive with the ATP-site directed labeling agents employed by these methods.

Currently, no assays combine the benefits of *in vitro* assays (high throughput) with those of *in vivo* approaches (relevant cellular context). We recently developed a quantitative protein-protein interaction assay to survey the association of the HSP90 chaperone and its CDC37 co-chaperone with the majority of human kinases *in vivo*¹. We established that one of the main determinants of HSP90's association with a particular kinase is the thermal stability of the kinase domain. Here, we exploit this finding and use HSP90 and CDC37 as thermodynamic sensors for profiling small molecule–kinase interactions in living cells. We further demonstrate that this assay is not limited to kinases as targets and HSP90 or CDC37 as sensors, suggesting a more general approach for probing small molecule–target interactions.

RESULTS

Characterizing ATP-competitive kinase inhibitors *in vivo*

To study HSP90–client protein interactions in a systematic manner, we developed an assay based on the LUMIER (LUminescence-based Mammalian IntERactome) assay¹³. Our implementation, LUMIER with bait control (BACON) both increases the assay throughput and enables quantitation of interactions¹. Briefly, the assay employs 293T cells stably expressing the chaperone protein HSP90 fused to *Renilla* luciferase. Plasmids encoding potential client proteins (e.g. kinases, transcription factors and ubiquitin ligases) with a 3xFLAG epitope tag are then transiently transfected into the luciferase-tagged HSP90 expressing cell line. The interaction of client proteins with the luciferase-tagged HSP90 is detected in cell lysates by immunoprecipitation with anti-FLAG antibodies in 384-well

plates and quantification of the luminescence signal from the luciferase-HSP90 fusion co-purified with the FLAG-tagged client proteins. Subsequently, client protein abundance is measured by ELISA, using a polyclonal anti-FLAG antibody. Finally, the quantitative interaction score is calculated as the ratio between the luminescence (chaperone abundance) and ELISA signals (client abundance) (Fig. 1A).

Previously, we found that small molecules targeting ABL kinase lead to a decrease in the interaction between BCR-ABL and HSP90¹. Small molecule binding stabilizes the kinase in its fully folded conformation and thereby decreases the concentration of the partially unfolded conformation that HSP90 recognizes with its cochaperone CDC37 (Fig. 1B). Here, we asked whether this method provides a means to assess the potencies of specific inhibitors quantitatively *in vivo*. To provide a well-studied test set, we measured the interaction of several BCR-ABL variants with HSP90 as a function of inhibitor concentration. Cells stably expressing the *Renilla*-HSP90 fusion were transfected with different BCR-ABL constructs and treated in triplicate with increasing concentrations of inhibitors for 1 hour before analysis. (Fig. 2A–D).

The potencies of each of the compounds in disrupting the HSP90 BCR-ABL interaction closely correlated with the known potencies of the compounds *in vivo*. Imatinib, the first-in-class BCR-ABL inhibitor that binds in the ATP pocket, displaced HSP90 from BCR-ABL with an EC₅₀ of 180 nM. Dasatinib, a second-generation inhibitor, was significantly more potent (EC₅₀: 6 nM)¹⁴. Neither inhibitor had an effect on the interaction between HSP90 and a BCR-ABL variant that carries an isoleucine-to-threonine substitution at residue 315 (T315I). The change in this “gatekeeper” residue of the ATP-binding pocket confers resistance to both inhibitors (Fig. 2B and 2C)¹⁴. By contrast, the third-generation inhibitor ponatinib (AP24534), specifically developed to combat the gatekeeper mutant¹⁵, not only affected the interaction of the native BCR-ABL with HSP90 but also of the BCR-ABL variant with the gatekeeper mutation. Moreover, in keeping with previous findings on the relative potency of the compound, ponatinib displaced the mutant protein from HSP90 with 5-fold lower potency (70 nM vs 22 nM) than it displaced the native BCR-ABL (Fig. 2D).

Kinase inhibitor treatment decreased the kinase–HSP90 interaction, without eliminating it completely. Many factors likely contribute to the residual binding in the presence of the inhibitor. First, the HSP90 chaperone cycle is complex and the client kinase may vary in its sensitivity to inhibitor at various points in its maturation¹. Second, the degree of thermal stabilization by a small molecule depends on many factors¹⁶ and even when a kinase is stabilized by a small molecule it will occasionally unfold and rebind HSP90. Finally, for some kinases the chaperone binding equilibrium might not be achieved in the 1h treatment we used. In any case, these factors should not change the EC₅₀ values derived from the assay.

In all of the above experiments, the compounds were added to the growth medium for one hour prior to cell lysis and the LUMIER assay. By contrast, the compounds had no effect on BCR-ABL–HSP90 interactions if they were added post lysis (Supplementary Fig. 1). Under the assay conditions we employed, once the cells are lysed, the HSP90 chaperone cycle is arrested due to low temperature, the absence of nucleotides and the presence of molybdate,

which is known to stabilize Hsp90-client interactions¹. Furthermore, it is unlikely that kinase inhibitors would bind the kinase when it is bound to HSP90 *in vitro*; structural studies suggest that the kinase is partially unfolded when bound to the chaperone complex¹⁷. Thus, although the assay readout occurs in lysates, it reflects the folding state of the kinase *in vivo* prior to lysis. The assay thus effectively measures the thermodynamic stabilization of the kinase fold in living cells.

Determining potencies of allosteric small molecule modulators

Allosteric inhibitors may be preferable to ATP-competitive inhibitors because their binding sites show a larger structural variability than the conserved ATP-binding site and therefore present much greater opportunities for achieving specificity. The difficulty of developing assays that accurately reflect *in vivo* kinase regulatory interactions has greatly hindered efforts to develop allosteric inhibitors. We therefore tested the ability of the HSP90–kinase interaction to quantitatively assess the effects of two reported allosteric modulators of the ABL kinase: GNF-2 and DPH^{18, 19}. Both compounds bind the myristate-binding (myr) pocket located in the C-terminal lobe of ABL (Fig. 3A), but they have opposing effects on ABL kinase activity: GNF-2 is an inhibitor, DPH an activator^{18, 19}.

Both GNF-2 and DPH displaced HSP90 from BCR-ABL with potencies in close agreement with their reported cellular potencies against BCR-ABL-dependent proliferation^{18–20} (Fig. 3A and 3B). Notably, the T315I mutation, located in the ATP-binding cleft and far from the myr-pocket, did not affect the ability of either compound to displace HSP90. By contrast, a point mutation (P465S) located in the myr-pocket virtually abolished the effect of GNF-2 and DPH on HSP90's interaction with BCR-ABL (Fig. 3C and 3D). Consistent with this, P465S confers strong resistance against GNF-2 *in vivo*¹⁸.

Another mutation in the myr-pocket (E505K) responded differently to GNF-2 and DPH. The E505K:HSP90 interaction was not sensitive to GNF-2, whereas it was sensitive to DPH (Fig. 3C and 3D). To date, no mutations have been reported to have distinct effects on allosteric modulators of ABL. To investigate the molecular basis of these results, we compared the published crystal structures of ABL bound to GNF-2 and to DPH^{18, 19}. In the GNF-2-bound conformation, Glu505 is adjacent to the myr-pocket, and E505K confers resistance against GNF-2 *in vivo* (Fig. 3E)¹⁸. In the DPH-bound conformation, the α I helix is extended, moving Glu505 away from the binding site¹⁹ (Fig. 3F). Pro465 is located in the mouth of the binding pocket in both conformations. Thus, our chaperone assay not only yields quantitative assessment of allosteric drug target binding affinities, but it can also provide evidence for qualitatively distinct binding modes.

Expanding the scope of the chaperone assay

About 40% of human kinases do not appreciably associate with HSP90¹, and therefore they cannot be currently assayed with our method. Might they be engineered to do so? In recognizing its clients, HSP90 does not bind particular sequence motifs but, rather, associates with intrinsically unstable kinase conformations. Yet, to be recognized as clients, the kinases must still have a recognizable kinase fold¹. Thus, mutations that globally destabilize the client would not likely work. We therefore introduced more strategic

causally linked to dominant Mendelian diseases (Supplementary Table 1). About 70% of these new constructs interacted with HSP90 and CDC37 and could thus be tested in our assay, compared to 60% of the original kinase panel.

First, we transfected our kinase collection into *Renilla*-HSP90 and CDC37-*Renilla* cells (each in duplicate) and quantitatively measured each kinase–HSP90 and kinase–CDC37 interaction by LUMIER with BACON. Consistent with our previous results¹, the assay was highly reproducible with an R^2 value of 0.98 between replicates (Fig. 5A and Supplementary Fig. 3). Next, we repeated the assay in quadruplicate, but treated the cells with 5 μ M staurosporine (2 replicates) or DMSO (2 replicates) for 1 hour prior to cell lysis. Staurosporine is a promiscuous kinase inhibitor targeting all kinase families⁴, and thus would be expected to affect a significant fraction of HSP90–kinase interactions. Indeed, staurosporine treatment led to a significant reduction in 45% of kinase–HSP90 interactions (Fig. 5B).

Having established the robustness and reproducibility of the assay platform, we then screened 30 small molecules at 5 μ M against our entire kinase collection. These included FDA-approved kinase inhibitors, inhibitors currently in clinical trials, and compounds in pre-clinical development (Supplementary Table 1). The compounds represented all types of kinase inhibitors: active (type I) and inactive (type II) conformation binders, allosteric (type III) modulators and irreversible inhibitors. HSP90 and CDC37 interaction profiles with kinases correlate very strongly¹ and the EC50 values derived with both interaction assays are nearly identical (see above), but the signal-to-noise ratio was slightly better with the CDC37-*Renilla* cell line (data not shown). Therefore, most inhibitors were profiled with CDC37 as the sensor (Supplementary Table 1).

In all but four cases, we identified the primary target of the inhibitor if it was among the HSP90- or CDC37-interacting kinases in our collection (Supplementary Table 1 and Supplementary Discussion). For example, chaperone profiling identified wild-type and mutant BRAF as specific targets of PLX4720 (Fig. 5C). Similarly, ponatinib has been reported as a potent BCR-ABL¹⁵, pan-FGFR²⁵, and FLT3 inhibitor²⁶. Consistent with this, we identified all three as prominent ponatinib targets (Fig. 5D). For PLX4720, we identified 17 additional kinases as potential targets and for ponatinib 48. It is possible that some of these represent indirect activities (e.g. upstream kinase activation) that could affect chaperone binding, but this is unlikely to be a general confounding factor. For example, receptor tyrosine kinase inhibitors did not affect the chaperone interactions of downstream kinases (e.g. MEK and ERK family kinases), even though their activity states must have been affected.

For all inhibitors, we measured inhibitor EC50 values for up to ten of the most significant kinase hits (see Supplementary Fig. 4 for examples and Supplementary Table 2 for all data). Previously established *in vitro* specificity profiles (KINOMEscan) were available for nine of the inhibitors^{5, 7}. For five of these (crizotinib, GDC0879, HG-6-64-1, PLX4720, and sorafenib), there was a statistically significant overlap between our data and previously published datasets (Supplementary Fig. 5). For two inhibitors (EPHB2 inhibitor ALW-II-49-7 and BTK inhibitor QL-X-138) the overlap was not statistically significant, as only a

few of the previously identified *in vitro* targets were profiled with our assay (Supplementary Fig. 5).

For staurosporine, a larger number of targets had been identified in previous *in vitro* investigations. To address this discrepancy, we chose six such kinases for further study. We transfected the kinases into 293T cells, treated cells with staurosporine, and asked whether staurosporine altered kinase autophosphorylation, a surrogate for kinase activity. For four of the six, autophosphorylation changes were consistent with our results from the primary screen (Supplementary Fig. 6A). Thus, for these kinases, our *in vivo* LUMIER assay reflect inhibitor specificity better than former *in vitro* assays. Autophosphorylation of one kinase was affected by the inhibitor, but when we retested it by LUMIER, it proved to be a *bona fide* target by this assay too. Thus, it was simply a false negative in the primary screen. Only one kinase, FLT4, showed a discordant pattern. It was not displaced from CDC37, even though its phosphotyrosine content decreased with staurosporine. Because we have found FLT4 to be a target of several other kinase inhibitors using our assay, this kinase is not intrinsically incompatible with the LUMIER assay. Instead, staurosporine might have an unusual mode of binding to FLT4 or the kinase might be transphosphorylated by a separate, staurosporine-sensitive kinase. Finally, we tested one kinase that was not previously identified as a staurosporine target but did score in our screen, JAK1. The effects of staurosporine on JAK1 autophosphorylation confirmed that it is indeed a target of this compound (Supplementary Fig. 6B). Thus, the chaperone interaction assay is a robust method for identifying biologically relevant kinase inhibitor targets in a high-throughput manner.

To more critically evaluate the relevance of our results to cellular physiology, we compared the measured EC50 values to previously published cellular potencies. We included only assays in which the cellular potency could be unequivocally attributed to a specific drug/target interaction (e.g. excluding sensitivity data for cancer cell lines that likely contain multiple genetic lesions). Such data were available for 40 drug/target pairs targeted by 10 diverse compounds (Supplementary Table 3). The cellular potency of these compounds spanned almost five orders of magnitude (100 pM to 5 μ M). Their measured EC50 values from the chaperone interaction assay strongly correlated with their cellular potencies (logarithmic R^2 0.74, $p < 0.0001$, linear R^2 0.59, $p < 0.0001$; Supplementary Fig. 7). The robust correlation between the two very different assays further demonstrates the ability of the LUMIER assay to address cellular physiology.

Kinome-wide profiling: Allosteric modulators

As noted above, allosteric kinase inhibitors are thought to be more specific than ATP-competitive inhibitors, as they target nonconserved pockets²⁷. Although this concept is intuitively reasonable, it has been challenging to systematically test it *in vivo*. To address this deficiency we used our chaperone sensor assay to profile six allosteric inhibitors and one allosteric activator. All proved to be exquisitely specific. For example, allosteric AKT inhibitors MK-2206 and Kin001-102, which bind the interface between the AKT kinase domain and its pleckstrin-homology (PH) domain²⁷, only targeted the AKT family kinases (Supplementary Figure 8). The allosteric MEK inhibitor trametinib did not affect any wild-

type kinases that interacted with CDC37. (Wild-type MEK1 (MAP2K1) or MEK2 (MAP2K2) do not associate with CDC37 and were not assayed.) However, introducing destabilizing mutations in MAPK2K2 led to robust CDC37 interaction, which was disrupted by trametinib (Supplementary Figure 8).

Finally, we assayed the two previously discussed compounds that target the ABL1 myr-pocket, GNF-2 and DPH. Again, ABL1 and BCR-ABL were the only kinases whose chaperone interactions were consistently affected by GNF-2 and DPH (Supplementary Fig. 9A and Supplementary Table 2). We also tested thirty-nine BCR-ABL variants that had been recovered in a screen for imatinib resistance²⁸. All but one of these were affected by GNF-2 treatment, but the extent of dissociation from HSP90 varied considerably (Supplementary Fig. 9B). Notably, nine of these variants had also been recovered in an independent screen for mutations that confer partial or full resistance to GNF-2 *in vivo*¹⁸. The GNF-2 resistant clones we profiled were less strongly displaced from HSP90 by GNF-2 than the remaining clones ($p < 0.0001$, Wilcoxon rank sum test; Supplementary Fig. 9B). The single variant whose interaction with HSP90 was not affected by GNF-2 (P439T/I502M) contained a mutation in the myr-pocket and had not previously been tested for GNF-2 resistance. To test the resistance of this variant in a biologically meaningful setting, we used BaF/3 cells that had been oncogenically transformed with this variant and were dependent on it for growth and survival. Indeed, as predicted by our assay, these cells were more resistant to GNF-2 than cells transformed with the native BCR-ABL (Supplementary Fig. 9C).

These results provide *in vivo* validation for the notion that allosteric modulators are more specific than ATP-competitive kinase inhibitors. Furthermore, the data show that drug-resistant variants can be predicted with high-throughput chaperone profiling.

Crizotinib is a potent inhibitor of ETV6-NTRK3

To demonstrate the translational value of our assay to uncover clinically relevant secondary targets, we focused on crizotinib (Xalkori®), a recently approved high-potency inhibitor of the ALK and MET tyrosine kinases²⁹. We identified several other tyrosine kinases as potential secondary targets (Supplementary Table 2). Some of these had been identified as secondary targets previously by other methods but *in vivo* data existed for only a few^{5, 7, 30}. To test the effect of crizotinib on the tyrosine kinase activity of the potential targets we identified, we assessed the autophosphorylation state of each kinase after a one-hour crizotinib treatment. As expected, crizotinib potently inhibited ALK autophosphorylation (Fig. 6A) as well as that of previously reported targets ABL1 and AXL (Supplementary Fig. 10). In addition, autophosphorylation of the translocation fusion kinase ETV6-NTRK3 was also markedly reduced by crizotinib (Fig. 6A). Although wild-type NTRK3 was among the 146 previously reported *in vitro* targets of the drug⁵, ETV6-NTRK3 fusion has previously not been described as an *in vivo* target of crizotinib. Other targets (FES, TESK1, INSR, EPHA2) were also affected by crizotinib, albeit only at higher concentrations (Supplementary Fig. 10). We also measured the EC50 of crizotinib for each target with the chaperone interaction assay. The potency of crizotinib in reducing kinase

autophosphorylation and its potency in dissociating the kinases from HSP90 were in good agreement (Fig. 6B and Supplementary Fig. 10).

Notably, crizotinib inhibited the ETV6-NTRK3 translocation fusion kinase in our assay even more potently (EC₅₀: 85 nM) than it inhibited its primary target ALK (EC₅₀: 220 nM) (Fig. 6B). This translocation has been found in pediatric tumors such as fibrosarcomas, mesoblastic nephromas and secretory breast carcinomas³¹. Infantile fibrosarcoma is the most common soft-tissue sarcoma in infants. Despite a generally favorable prognosis, treatment of more advanced tumors can require radical surgery and even amputation³². In adults, this translocation has been associated with acute myeloid leukemia^{33, 34} and a distinct subclass of salivary gland tumors, which occasionally metastasize and have poor outcome^{33–35}. Thus, a drug targeting ETV6-NTRK3 might offer a valuable treatment option for these rare but often devastating cancers.

To test the effect of crizotinib on human tumor cells, we chose the M091 cell line, which carries the ETV6-NTRK3 translocation and was derived from a patient with acute myeloid leukemia³⁶. Confirming our results from 293T cells, crizotinib potently inhibited endogenous ETV6-NTRK3 autophosphorylation in M091 cells after 1h treatment (Fig. 6C). To determine if crizotinib inhibited signaling downstream of activated NTRK3, we measured the effect of crizotinib on ERK phosphorylation³⁷. ERK phosphorylation was reduced in a concentration-dependent manner upon drug treatment (Fig. 6C).

Next, we assayed the sensitivity of M091 cell growth and survival to crizotinib. The cells were very sensitive to the drug, with a GI₅₀ in the low nanomolar range (Fig. 6D). To exclude the possibility that this was due to inhibition of other known crizotinib targets that could play an important role in M091 biology, we tested three additional inhibitors. NVP-TAE684 inhibits ALK with low nanomolar potency³⁸. Yet, it inhibited M091 cell growth only at micromolar concentrations (Fig. 6D), suggesting that ALK inhibition is not responsible for crizotinib's growth-inhibitory effect. Similarly, the ABL1 inhibitor imatinib had no effect on M091 proliferation even at high concentrations (Fig. 6D). However, another ABL1 inhibitor ponatinib, which we found to also target NTRK3 in our screen, (Supplementary Table 2), did inhibit the growth of the cells with nanomolar potency. Thus, the effect of crizotinib on M091 cell proliferation is not due to ALK or ABL1 inhibition but is very likely a result of direct inhibition of ETV6-NTRK3.

To evaluate the activity of crizotinib *in vivo* against an ETV6-NTRK3-dependent tumor, we developed a xenograft model in non-obese diabetic-severe combined immunodeficiency (NOD-SCID) mice. Parental M091 cells were passaged as subcutaneous implants through these mice to generate a more highly tumorigenic variant that was adapted to engraft and progress in sufficiently uniform fashion to support testing of drug activity *in vivo*. When explanted in cell culture, these *in vivo*-passaged cells (M091-TA) remained highly sensitive to crizotinib (Supplementary Fig. 11) and were used for subsequent experiments evaluating anticancer activity. Three weeks after subcutaneous injection of M091-TA cells, we randomly assigned mice bearing established xenografts to treatment with crizotinib or vehicle control. Crizotinib was administered by oral gavage using a well-tolerated dose of 50 mg/kg once a day. The control treatment group received an equal volume of water on the

same schedule. Control-treated tumors rapidly grew to the point where the mice had to be sacrificed. In contrast, crizotinib induced tumor regression after only a few days' treatment (Fig. 6E).

At the end of the treatment interval, we resected tumor xenografts to examine relevant pharmacodynamic endpoints. Control-treated samples showed dense sheets of tumor cells with overt features of high-grade malignancy: large irregular nuclei with prominent nucleoli, regions of nuclear clearing representing open chromatin, and frequent, easily identified mitotic figures (Fig. 6F). By contrast, in crizotinib-treated animals tumor cells were sparse and were embedded in a fibrotic extracellular matrix. Mitoses were very infrequent, nucleoli were inconspicuous and nuclei were small with condensed chromatin, all features of non-proliferating cells (Fig. 6F). Immunohistochemistry (IHC) for two proliferation markers, Ki67 (MIB1) and phospho-histone H3S10, confirmed that crizotinib treatment had markedly reduced proliferation (Fig. 6F and Supplementary Fig. 12). Moreover, crizotinib treatment caused a sharp decrease in totalphosphotyrosine levels in the tumors (Supplementary Fig. 12) and specifically in the activated form of STAT3 that is phosphorylated in cells carrying the ETV6-NTRK3 translocation (Fig. 6F)³⁹.

DISCUSSION

Here, we establish that chaperones can be used as 'thermodynamic sensors' for drug-target interactions. We use HSP90, CDC37 and HSC70 as examples of chaperones, and kinases and steroid hormone receptors as examples of drug targets. But it is likely that our approach will prove broadly applicable with other chaperones and other drug targets. The binding of small molecules to their targets generally leads to thermodynamic stabilization of those targets⁴⁰. If the target proteins are in equilibrium between their fully folded and partially folded chaperone-bound conformations, drug binding will lead to decreased chaperone association. Chaperones associate with a large fraction of proteins in all organisms even at their steady states^{1, 41, 42}, and, as we have shown, proteins that do not associate with them in this manner can be readily engineered to do so.

Our assay does not depend on the enzymatic activity of the target protein nor on a particular binding pocket in the target. Thus, it should be well suited for the pursuit of drugs for targets that have been notoriously difficult to assay in biologically relevant contexts, including E3 ligases¹, transcription factors¹, and diverse protein-protein interactions. Our method is amenable to high-throughput automation, bridging the gap between the more traditional high-throughput *in vitro* methods and lower throughput *in vivo* approaches in drug discovery.

We illustrated the utility of chaperone profiling by surveying kinase inhibitor specificities *in vivo*. Compared to other available methods for kinase inhibitor profiling⁵⁻⁷, our approach has several advantages. First, it uses full-length kinases in their native cellular environment, in the context of physiological post-translational modifications, conformational switches, and cellular interactors. Although the expression levels of the kinases in our assay are higher than endogenous levels, the strong correlation between our results and *in vivo* potency suggests that this is not a generally confounding factor. With the use of lentiviral delivery

systems it should be readily adaptable to any cell type in cases where a particular cellular context is required (e.g. stem cells, neuronal cells). Second, kinases are assayed at physiological ATP concentrations. As most kinase inhibitors are ATP-competitive, the difference between *in vitro* and *in vivo* ATP concentrations often leads to substantial changes in cellular potency. Third, the assay is compatible with allosteric inhibitors and activators, in contrast to other *in vivo* approaches^{11, 12}. For example, neither GNF-2 nor MK2206 would have been identified in an *in vitro* screen using ABL1 or AKT1 kinase domains only, as the inhibitors absolutely require the kinases' regulatory domains for function²⁷.

Finally, we established that the assay can be used to discover clinically relevant drug targets. NTRK3 and its translocation fusion variant ETV6-NTRK3 proved to be prominent targets of crizotinib. Crizotinib inhibits ETV6-NTRK3 with nanomolar potency and treatment of ETV6-NTRK3-dependent xenografts with crizotinib leads to dramatic regression of tumors. These results suggest that it might be worth testing crizotinib as a therapeutic agent against cancers driven by the ETV6-NTRK3 translocation. Crizotinib already is already approved for use in the treatment of certain lung cancers. Recommended dosing parameters with a good safety profile for children have already been established⁴³. Thus it should be possible to translate these findings rapidly to efficacy trials in selected pediatric malignancies such as infantile fibrosarcoma. Furthermore, given the intense interest in repurposing drugs and expanding the scope of druggable targets, the ease and reproducibility of our assay should have broad application in drug development.

METHODS

Kinase clones

The majority of the kinase collection has been described previously¹. Additional kinases were amplified from cDNA and cloned into pDONR221 entry vector, and subsequently transferred into a pcDNA3.1-based expression vector with a CMV promoter and a C-terminal 3xFLAG-V5 tag, using Gateway LR clonase. Kinase mutants were created with site-directed mutagenesis, except for BCR-ABL alleles, which were amplified from retroviral vectors (kindly provided by M. Azam) and cloned into the expression vector with Gateway cloning. All mutations were verified by Sanger sequencing. Coordinates for the translocation breakpoints were downloaded from TICdb⁴⁴ and the translocations were created with fusion PCR⁴⁵. Translocation breakpoints were verified by Sanger sequencing.

LUMIER with BACON and inhibitor profiling

LUMIER with BACON was performed as previously described¹. To assay compound EC50 values, 3xFLAG tagged kinases (or steroid hormone receptors) were transfected into stable 293T reporter cell lines (*Renilla*-HSP90AB1, *CDC37*-*Renilla* or *Renilla*-HSPA8) in 6-well or 12-well plate format. Next day, the cells were split into 96-well plates, and 24 hours later the cells were treated with a 3-fold dilution series of the inhibitor in triplicate for 1 hour prior to cell lysis and the LUMIER assay.

Renilla-HSP90AB1 and CDC37-*Renilla* cell lines have been described earlier¹. The stable polyclonal 293T cell line expressing *Renilla*-HSPA8 was created with lentiviral infection. The expression construct contained a codon-optimized *Renilla* luciferase fused to the N terminus of human HSPA8 (Hsc70), separated by a glycine-serine rich linker.

To profile kinase inhibitor specificities, each kinase was transfected into the reporter cell line in quadruplicate using polyethylenimine (branched PEI, Sigma-Aldrich 408727). Two days after transfection, two sets of transfections were treated with 5 μ M inhibitor and two with vehicle (DMSO) only for 1 hour. LUMIER assay was performed on 384-well plates as previously described¹.

Statistical analysis

The quantitative chaperone–client interaction was calculated as the \log_2 [luminescence]- \log_2 [ELISA], and normalized such that weakest interactions had an interaction score of 0–1. Kinases for which the luminescence from Hsp90 or Cdc37 was weaker than two-fold over negative control (3xFLAG-tagged EGFP) were classified as non-interactors and excluded from analysis.

Kinase inhibitor profiling data was analyzed with the Bioconductor package in R. Duplicate datasets were median-normalized and differential response in treated vs control samples was assayed by a moderated t-test as implemented in the limma package in R. Kinases were classified as inhibitor targets if the change in Hsp90 or Cdc37 interaction upon inhibitor treatment was statistically significant ($p < 0.005$). Compounds that bind the fully folded kinase domain are not expected to increase kinase–chaperone interactions; rather, these events represent variation (noise) in the assay. Therefore, if there were more than three kinases that increased their interaction with Hsp90 or Cdc37 upon drug addition with the $p < 0.005$ cutoff, a more stringent cutoff of $p < 0.001$ was applied.

BaF/3 cell proliferation assay

The IL-3–dependent murine pro-B cell line Ba/F3 was maintained in RPMI-1640 medium supplemented with 10% FBS and 10 U/mL recombinant murine IL-3 (Roche). Mutant BCR-ABL–expressing Ba/F3 cells were generated as previously described⁴⁶. Wild-type BCR-ABL–expressing Ba/F3 cells and mutant BCR-ABL–expressing cell lines were maintained in RPMI-1640 medium with 10% FBS. For cellular proliferation assays, cells (0.4×10^6 /mL) were plated in duplicate in 96-well plates containing increasing drug concentrations (0.005–10 μ M). After incubation at 37 °C in 5% CO₂ for 48 hours, the effect of the compounds on cell viability was determined by the CellTiter Glo cell viability assay (Promega).

Xenografts

Tumor volumes (mm^3) were calculated by measuring the length (long dimension in centimeters) and width (short dimension) of each mass with a caliper and then using the following standard formula to estimate volume: (length \times width \times width) \times 0.52 \times 1000. Tumor size was measured by a lab technical research associate who was blinded to the treatment groups.

Experimental groups consisted of 8 mice per treatment. Cells were inoculated subcutaneously via 27g needle in a 50/50 mix of PBS and Matrigel in the right inguinal region of each mouse. Daily treatment was begun about 3 weeks later when the average tumor volume across mice had reached ~350 mm³. Mice were treated orally with crizotinib using a gavage needle as per standard practice.

Immunohistochemistry

Tissue sections were deparaffinized and rehydrated through xylene and graded alcohols. Endogenous peroxidase activity was quenched by incubating the sections 15 minutes with 3% hydrogen peroxide in 100% alcohol (1:1). Antigen retrieval was performed with Dako target retrieval solution, pH 6.0 (citrate) or 8.0 (EDTA) in pressure cooker (120°C+/-2°C) for 30 seconds at 15+/-5 psi. Sections were incubated for either 40 minutes at room temperature (Ki67, phospho-tyrosine) or 4°C overnight (pSTAT3 Y705, phospho-histone H3S10). Application of the secondary antibodies was followed by incubation for 30 minutes with Dako Labeled Polymer-HRP goat anti-rabbit IgG for all of above antibodies except phospho-tyrosine for which M.O.M kit was applied (Vector laboratories, PK-2200). The sections were then visualized with 3, 3'-diaminobenzidine (DAB)+substrate-chromogen which results in a brown-colored precipitate at the antigen site. Mayer hematoxylin was used for counterstaining.

Reagents

Kinase inhibitors were purchased from Chemietek (Indianapolis, IN), Selleck (Houston, TX), Sigma-Aldrich (St. Louis, MO), or synthesized in the Gray laboratory. All inhibitors were dissolved in DMSO. Antibodies were purchased from Sigma (anti-FLAG M2 F1804, anti-FLAG M2 affinity resin F2426), Santa Cruz (anti-TrkC N-13 sc-47520), Cell Signaling (anti-pTyr 9411; anti-pErk 4370, anti-Erk 4695), and Abcam (anti-DDDDK ab1278).

Supplementary Material

Refer to Web version on PubMed Central for supplementary material.

Acknowledgments

We thank the Lindquist lab members for valuable discussions and comments on the manuscript. We also thank Mohammed Azam (Cincinnati Children's Hospital Medical Center) for providing mutant BCR-ABL clones and Prat Thiru, Inma Barrasa and George Bell (Whitehead Institute) for help with primer design and statistical analysis. M.T. was supported by Human Frontier Science Programme long-term fellowship. S.L. is a Howard Hughes Medical Institute investigator. Support for this study was also provided by the NIH Genomics Based Drug Discovery-Driving Medical Projects grant UL1-DE019585, administratively linked to NIH grants RL1-GM084437, RL1-CA133834, and RL1-HG004671.

References

1. Taipale M, et al. Quantitative analysis of HSP90-client interactions reveals principles of substrate recognition. *Cell*. 2012; 150:987–1001. [PubMed: 22939624]
2. Goldstein DM, Gray NS, Zarrinkar PP. High-throughput kinase profiling as a platform for drug discovery. *Nat Rev Drug Discov*. 2008; 7:391–397. [PubMed: 18404149]
3. Karaman MW, et al. A quantitative analysis of kinase inhibitor selectivity. *Nat Biotechnol*. 2008; 26:127–132. [PubMed: 18183025]

4. Fabian MA, et al. A small molecule-kinase interaction map for clinical kinase inhibitors. *Nat Biotechnol.* 2005; 23:329–336. [PubMed: 15711537]
5. Davis MI, et al. Comprehensive analysis of kinase inhibitor selectivity. *Nature biotechnology.* 2011; 29:1046–1051.
6. Fedorov O, et al. A systematic interaction map of validated kinase inhibitors with Ser/Thr kinases. *Proc Natl Acad Sci U S A.* 2007; 104:20523–20528. [PubMed: 18077363]
7. Anastasiadis T, Deacon SW, Devarajan K, Ma H, Peterson JR. Comprehensive assay of kinase catalytic activity reveals features of kinase inhibitor selectivity. *Nature biotechnology.* 2011; 29:1039–1045.
8. Bain J, et al. The selectivity of protein kinase inhibitors: a further update. *Biochem J.* 2007; 408:297–315. [PubMed: 17850214]
9. Eck MJ, Manley PW. The interplay of structural information and functional studies in kinase drug design: insights from BCR-Abl. *Current opinion in cell biology.* 2009; 21:288–295. [PubMed: 19217274]
10. Posy SL, et al. Trends in kinase selectivity: insights for target class-focused library screening. *Journal of medicinal chemistry.* 2011; 54:54–66. [PubMed: 21128601]
11. Bantscheff M, et al. Quantitative chemical proteomics reveals mechanisms of action of clinical ABL kinase inhibitors. *Nat Biotechnol.* 2007; 25:1035–1044. [PubMed: 17721511]
12. Patricelli MP, et al. In situ kinase profiling reveals functionally relevant properties of native kinases. *Chem Biol.* 2011; 18:699–710. [PubMed: 21700206]
13. Barrios-Rodiles M, et al. High-throughput mapping of a dynamic signaling network in mammalian cells. *Science.* 2005; 307:1621–1625. [PubMed: 15761153]
14. Shah NP, et al. Overriding imatinib resistance with a novel ABL kinase inhibitor. *Science.* 2004; 305:399–401. [PubMed: 15256671]
15. O'Hare T, et al. AP24534, a pan-BCR-ABL inhibitor for chronic myeloid leukemia, potently inhibits the T315I mutant and overcomes mutation-based resistance. *Cancer Cell.* 2009; 16:401–412. [PubMed: 19878872]
16. Waldron TT, Murphy KP. Stabilization of proteins by ligand binding: application to drug screening and determination of unfolding energetics. *Biochemistry.* 2003; 42:5058–5064. [PubMed: 12718549]
17. Vaughan CK, et al. Structure of an Hsp90-Cdc37-Cdk4 complex. *Mol Cell.* 2006; 23:697–707. [PubMed: 16949366]
18. Zhang J, et al. Targeting Bcr-Abl by combining allosteric with ATP-binding-site inhibitors. *Nature.* 2010; 463:501–506. [PubMed: 20072125]
19. Yang J, et al. Discovery and characterization of a cell-permeable, small-molecule c-Abl kinase activator that binds to the myristoyl binding site. *Chem Biol.* 2011; 18:177–186. [PubMed: 21338916]
20. Iacob RE, Zhang J, Gray NS, Engen JR. Allosteric interactions between the myristate- and ATP-site of the Abl kinase. *PLoS One.* 2011; 6:e15929. [PubMed: 21264348]
21. Xu W, et al. Surface charge and hydrophobicity determine ErbB2 binding to the Hsp90 chaperone complex. *Nat Struct Mol Biol.* 2005; 12:120–126. [PubMed: 15643424]
22. Picard D. Chaperoning steroid hormone action. *Trends in endocrinology and metabolism: TEM.* 2006; 17:229–235. [PubMed: 16806964]
23. Couture P, Theriault C, Simard J, Labrie F. Androgen receptor-mediated stimulation of 17 beta-hydroxysteroid dehydrogenase activity by dihydrotestosterone and medroxyprogesterone acetate in ZR-75-1 human breast cancer cells. *Endocrinology.* 1993; 132:179–185. [PubMed: 8380373]
24. Adcock IM, Nasuhara Y, Stevens DA, Barnes PJ. Ligand-induced differentiation of glucocorticoid receptor (GR) trans-repression and transactivation: preferential targetting of NF-kappaB and lack of I-kappaB involvement. *British journal of pharmacology.* 1999; 127:1003–1011. [PubMed: 10433509]
25. Gozgit JM, et al. Ponatinib (AP24534), a Multitargeted Pan-FGFR Inhibitor with Activity in Multiple FGFR-Amplified or Mutated Cancer Models. *Mol Cancer Ther.* 2012; 11:690–699. [PubMed: 22238366]

26. Gozgit JM, et al. Potent activity of ponatinib (AP24534) in models of FLT3-driven acute myeloid leukemia and other hematologic malignancies. *Mol Cancer Ther.* 2011; 10:1028–1035. [PubMed: 21482694]
27. Dar AC, Shokat KM. The evolution of protein kinase inhibitors from antagonists to agonists of cellular signaling. *Annual review of biochemistry.* 2011; 80:769–795.
28. Azam M, Latek RR, Daley GQ. Mechanisms of autoinhibition and STI-571/imitinib resistance revealed by mutagenesis of BCR-ABL. *Cell.* 2003; 112:831–843. [PubMed: 12654249]
29. Kwak EL, et al. Anaplastic lymphoma kinase inhibition in non-small-cell lung cancer. *N Engl J Med.* 2010; 363:1693–1703. [PubMed: 20979469]
30. Zou HY, et al. An orally available small-molecule inhibitor of c-Met, PF-2341066, exhibits cytoreductive antitumor efficacy through antiproliferative and antiangiogenic mechanisms. *Cancer research.* 2007; 67:4408–4417. [PubMed: 17483355]
31. Lannon CL, Sorensen PH. ETV6-NTRK3: a chimeric protein tyrosine kinase with transformation activity in multiple cell lineages. *Semin Cancer Biol.* 2005; 15:215–223. [PubMed: 15826836]
32. Orbach D, et al. Infantile fibrosarcoma: management based on the European experience. *J Clin Oncol.* 2010; 28:318–323. [PubMed: 19917847]
33. Eguchi M, et al. Fusion of ETV6 to neurotrophin-3 receptor TRKC in acute myeloid leukemia with t(12;15)(p13;q25). *Blood.* 1999; 93:1355–1363. [PubMed: 9949179]
34. Kralik JM, et al. Characterization of a newly identified ETV6-NTRK3 fusion transcript in acute myeloid leukemia. *Diagn Pathol.* 2011; 6:19. [PubMed: 21401966]
35. Skalova A, et al. Mammary analogue secretory carcinoma of salivary glands, containing the ETV6-NTRK3 fusion gene: a hitherto undescribed salivary gland tumor entity. *Am J Surg Pathol.* 2010; 34:599–608. [PubMed: 20410810]
36. Okabe M, et al. Megakaryocytic differentiation of a leukemic cell line, MC3, by phorbol ester: induction of glycoprotein IIb/IIIa and effects on expression of IL-6, IL-6 receptor, mpl and GATA genes. *Leuk Res.* 1995; 19:933–943. [PubMed: 8632663]
37. Tognon C, et al. The chimeric protein tyrosine kinase ETV6-NTRK3 requires both Ras-Erk1/2 and PI3-kinase-Akt signaling for fibroblast transformation. *Cancer research.* 2001; 61:8909–8916. [PubMed: 11751416]
38. Galkin AV, et al. Identification of NVP-TAE684, a potent, selective, and efficacious inhibitor of NPM-ALK. *Proceedings of the National Academy of Sciences of the United States of America.* 2007; 104:270–275. [PubMed: 17185414]
39. Gadd S, et al. Mediators of receptor tyrosine kinase activation in infantile fibrosarcoma: a Children's Oncology Group study. *J Pathol.* 2012; 228:119–130. [PubMed: 22374738]
40. Chaires JB. Calorimetry and thermodynamics in drug design. *Annual review of biophysics.* 2008; 37:135–151.
41. Gong Y, et al. An atlas of chaperone-protein interactions in *Saccharomyces cerevisiae*: implications to protein folding pathways in the cell. *Mol Syst Biol.* 2009; 5:275. [PubMed: 19536198]
42. Kerner MJ, et al. Proteome-wide analysis of chaperonin-dependent protein folding in *Escherichia coli*. *Cell.* 2005; 122:209–220. [PubMed: 16051146]
43. Mosse YP, et al. Efficacy of crizotinib in children with relapsed/refractory ALK-driven tumors including anaplastic large cell lymphoma and neuroblastoma: A Children's Oncology Group phase I consortium study. *Journal of Clinical Oncology.* 2012 Supplement, Abstract 9500.
44. Novo FJ, de Mendibil IO, Vizmanos JL. TICdb: a collection of gene-mapped translocation breakpoints in cancer. *BMC Genomics.* 2007; 8:33. [PubMed: 17257420]
45. Atanassov II, Etechells JP, Turner SR. A simple, flexible and efficient PCR-fusion/Gateway cloning procedure for gene fusion, site-directed mutagenesis, short sequence insertion and domain deletions and swaps. *Plant Methods.* 2009; 5:14. [PubMed: 19863796]
46. Koh EY, Chen T, Daley GQ. Novel retroviral vectors to facilitate expression screens in mammalian cells. *Nucleic acids research.* 2002; 30:e142. [PubMed: 12490733]

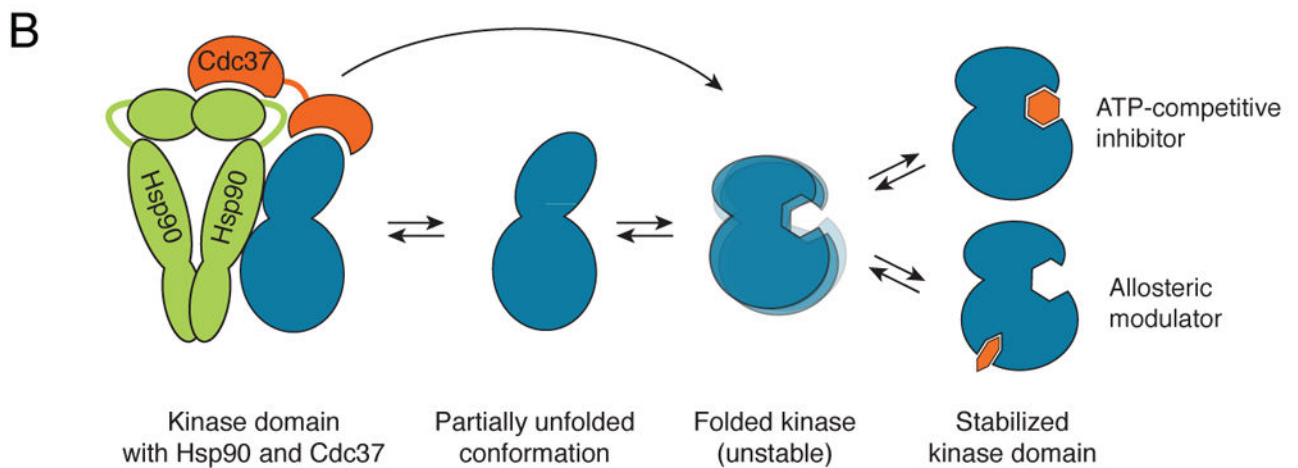
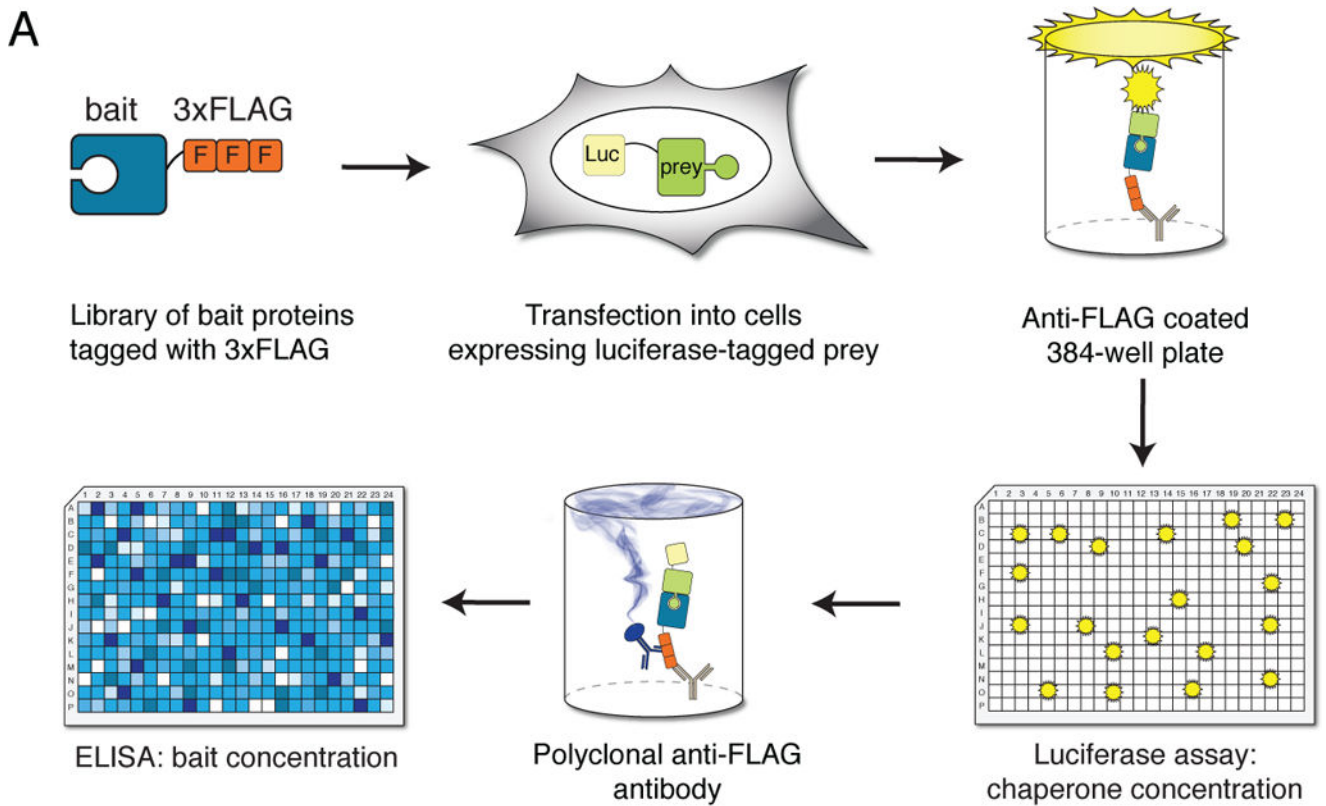


Figure 1. Principle of the chaperone assay

(a) LUMIER with BACON assay. Chaperone-*Renilla* luciferase fusion protein is stably expressed in 293T cells. 3xFLAG-tagged bait proteins are transfected into the cell line in 96-well format, and the cell lysates expressing each bait protein are applied to anti-FLAG coated 384-well plates. The amount of luminescence in the well after washing off nonspecifically binding proteins indicates the amount of co-purified chaperone. After the luminescence measurement, the amount of bait protein is measured with ELISA, using a

different, polyclonal anti-FLAG antibody coupled to horseradish peroxidase. The interaction score is calculated as $\log_2[\text{chaperone/bait}]$.

(b) Protein kinases are in equilibrium between the fully folded conformation and a partially unfolded conformation that is recognized by Hsp90 and its kinase-specific cochaperone Cdc37. Hsp90 machinery assists the kinase in adopting its fully folded conformation. Binding of a small molecule to the kinase fold shifts the equilibrium towards the fully folded conformation, which can be detected as decreased chaperone interaction.

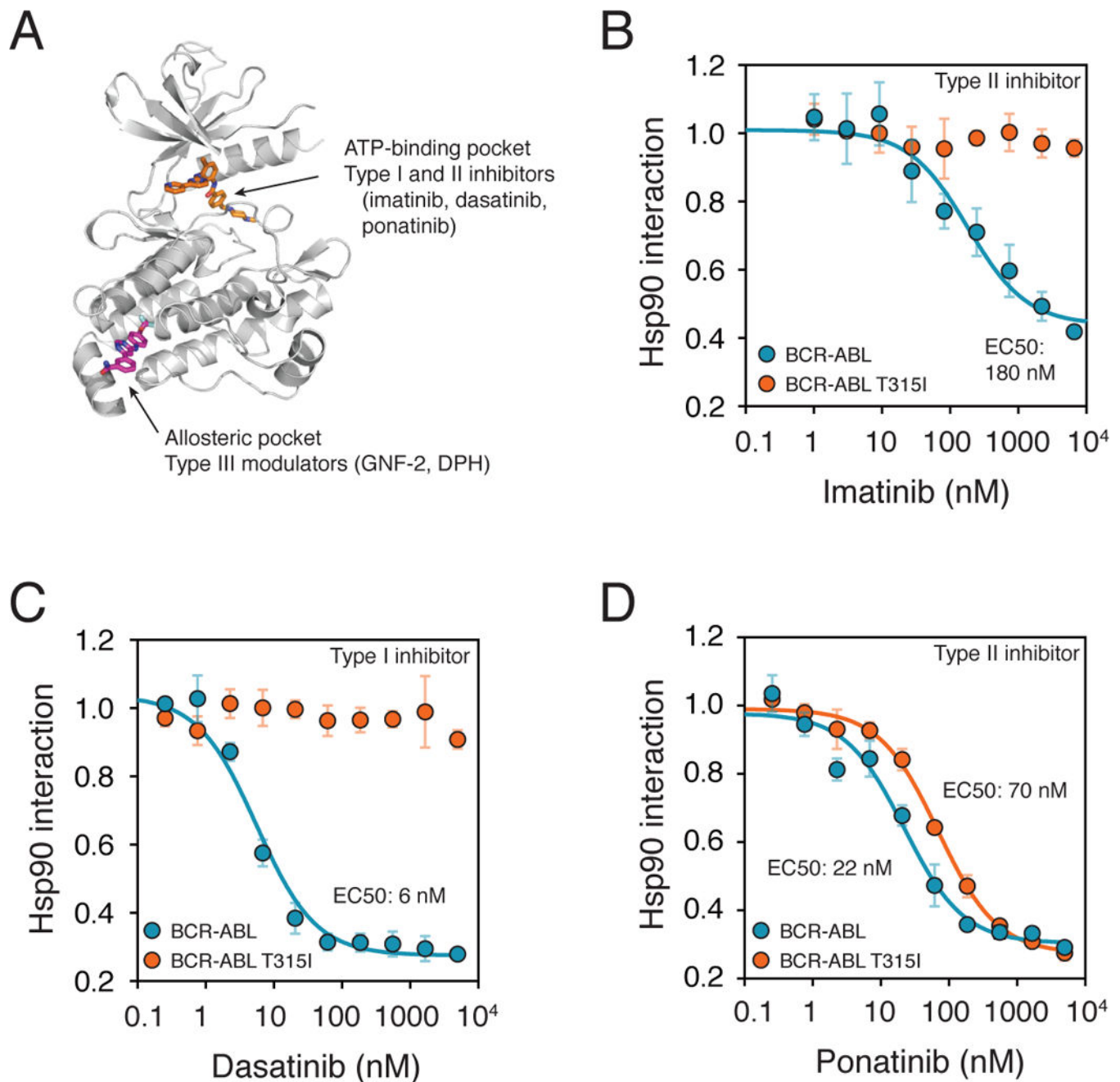


Figure 2. Characterization of ATP-competitive ABL inhibitor potencies with the chaperone interaction assay

(a) ABL1 and BCR-ABL can be targeted by two distinct mechanisms. Type I and II ATP-competitive inhibitors, such as imatinib (orange), bind the ATP-binding cleft, whereas allosteric modulators (type III; GNF-2, magenta) bind the myristate-binding pocket in the kinase C-terminal lobe. Figure adapted from PDB entry 3K5V.

(b–d) Analysis of kinase inhibitor potencies with the chaperone interaction assay. 3xFLAG-tagged native BCR-ABL and the gatekeeper mutant T315I were transfected into 293T cells stably expressing *Renilla* luciferase-Hsp90 fusion protein. Cells were treated with increasing

concentrations of inhibitors for 1 hour prior to cell lysis and the LUMIER assay. Treatment of cells with type II inhibitors imatinib (**b**) and ponatinib (**d**) or type I inhibitor dasatinib (**c**) lead to decreased BCR-ABL–HSP90 interaction. To obtain inhibitor EC50 values, relative Hsp90 interaction values (no inhibitor = 1) were fitted to a three-parameter dissociation curve with Graphpad Prism. Error bars indicate standard deviation.

Author Manuscript

Author Manuscript

Author Manuscript

Author Manuscript

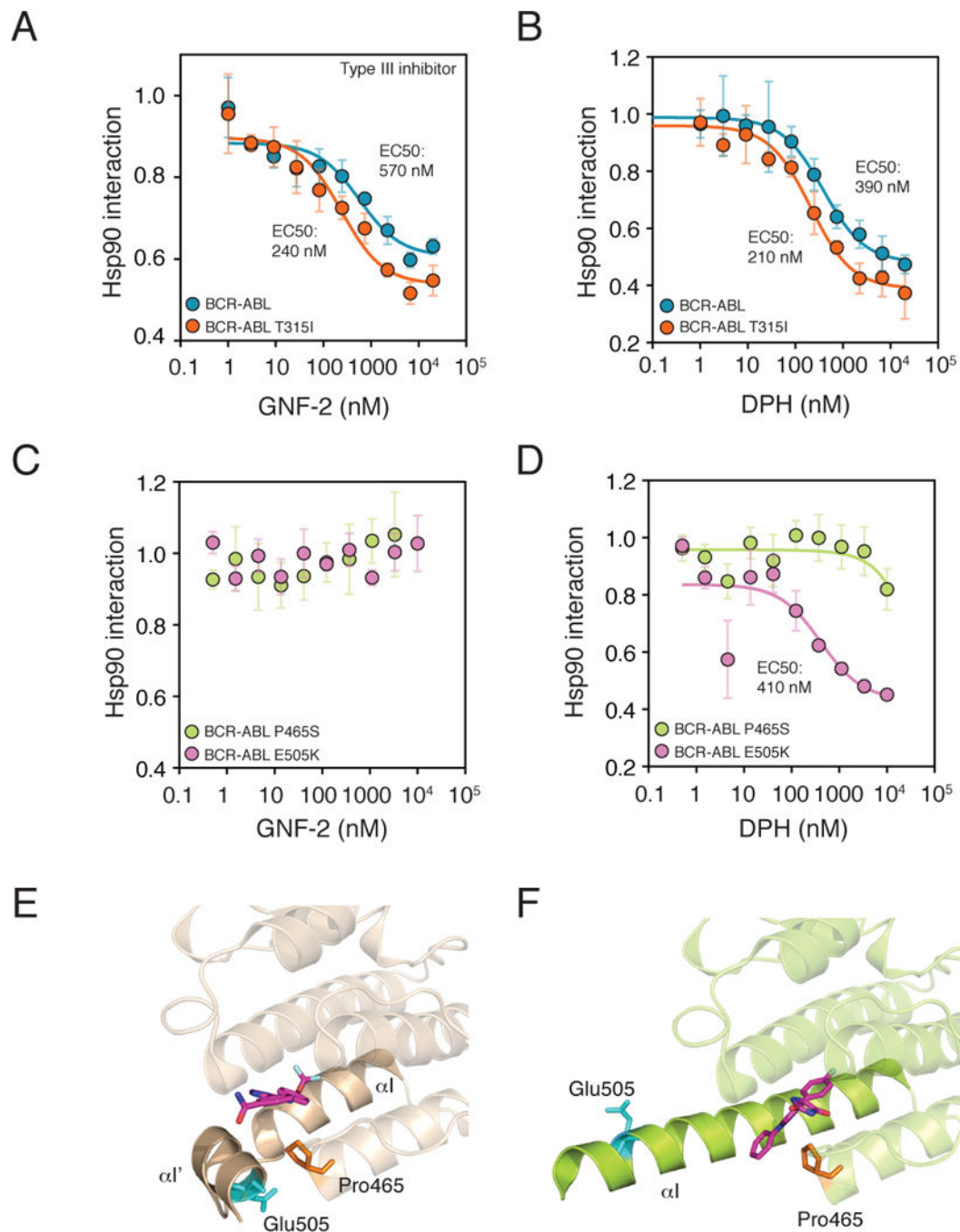


Figure 3. Characterizing allosteric ABL modulators with the chaperone interaction assay (a–d) Analysis of kinase inhibitor potencies with the chaperone interaction assay. 3xFLAG-tagged native BCR-ABL and its mutant variants transfected into 293T cells stably expressing *Renilla* luciferase-Hsp90 fusion protein. Cells were treated with increasing concentrations of inhibitors for 1 hour prior to cell lysis and the LUMIER assay. Allosteric compounds GNF-2 (an inhibitor) and DPH (an activator) displace HSP90 from both the native BCR-ABL and the gatekeeper mutant T315I (a–b). In contrast, mutations in the allosteric myristate-binding pocket have distinct effects on DPH and GNF-2 (c–d). P465S

confers resistance against both DPH and GNF-2, whereas E505K confers resistance against only GNF-2. Error bars indicate standard deviation.

(e–f) Structural analysis of ABL illuminates the distinct effects of myr-pocket mutations P465S and E505K on GNF-2 and DPH. In the GNF-2-bound autoinhibited conformation **(e)**, ABL1 α I helix (solid, champagne-colored helix) is bent 90°, bringing Glu505 (cyan) to close proximity with the myristate-binding pocket where GNF-2 (magenta) binds. Pro465 (orange) is located in the mouth of the binding pocket. The structure is based on PDB entry 3K5V. In the DPH-bound conformation **(f)**, α I (solid green helix) is extended and Glu505 (cyan) is solvent-accessible. In contrast, Pro465 (orange) is in the same conformation as in the GNF-2 bound state. DPH, magenta. The structure is based on PDB entry 3PYY.

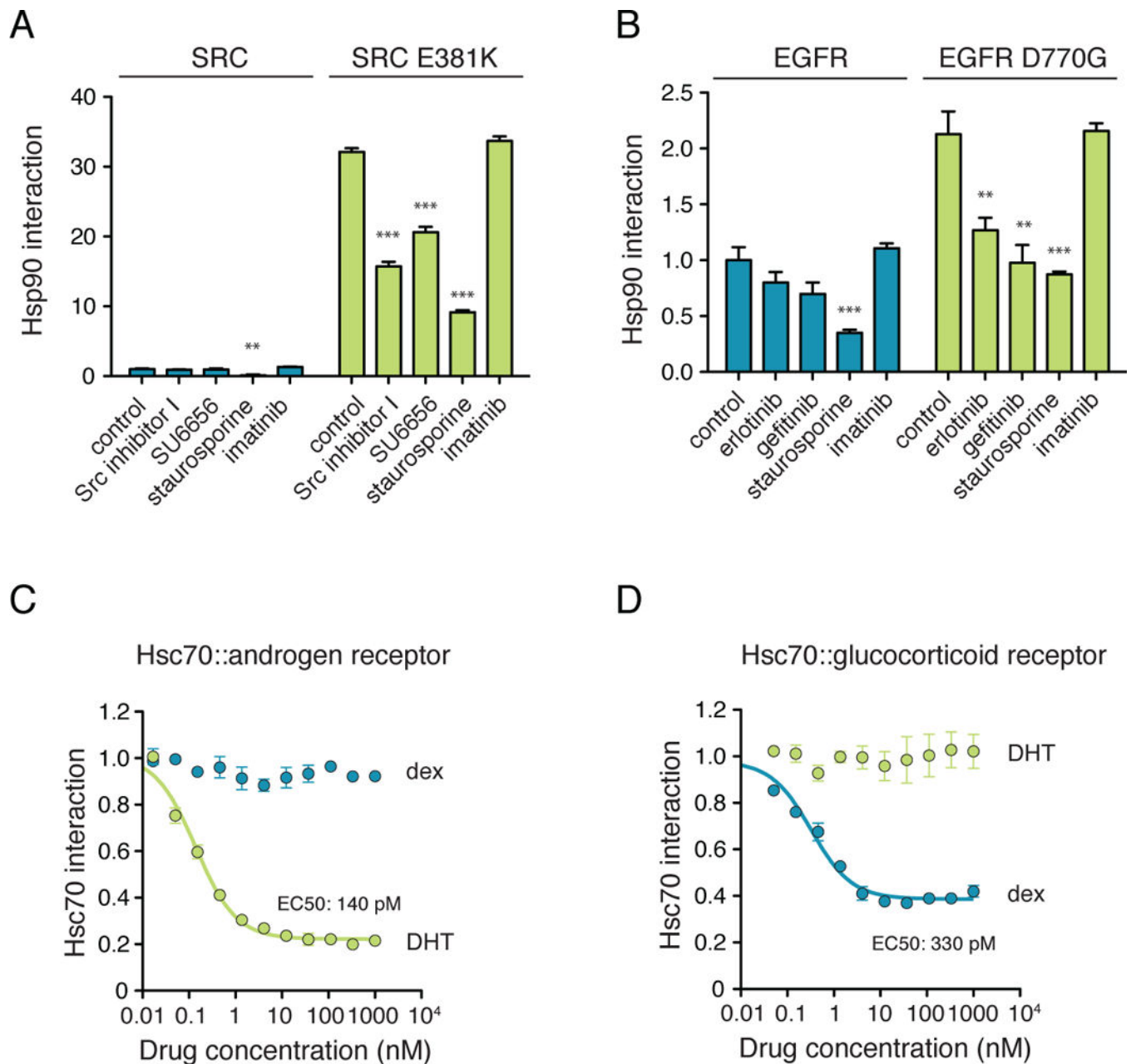


Figure 4. Expanding the scope of the chaperone interaction assay

(a) SRC does not appreciably associate with HSP90 in LUMIER assay, and thus, binding of the SRC-specific inhibitors SU6656 and Src inhibitor I to the kinase cannot be measured with LUMIER. Increasing SRC–HSP90 interaction by introducing a point mutation (E381K) to SRC kinase domain enables the detection of SU6656 and Src inhibitor I binding to the kinase. Inhibitors (10 μ M) were added to the cells for 1h prior to cell lysis and the LUMIER assay. Interaction scores correspond to relative interactions (Wild type SRC with no inhibitor = 1) \pm SD (n=4). Statistical test for significance was unpaired t-test with unequal variance. **, $p < 0.01$; ***, $p < 0.001$.

(b) Wild-type EGFR associates with HSP90 only weakly. Increasing its interaction with HSP90 with an aspartic acid-to-glycine mutation (D770G) facilitates the detection of binding of the EGFR-specific inhibitors erlotinib and gefitinib to EGFR. Experiment was performed as in **(a)**. **, $p < 0.01$; ***, $p < 0.001$.

(c–d) 293T cells stably expressing Renilla-Hsc70 (HSPA8) were transfected with 3xFLAG tagged androgen receptor **(c)** or glucocorticoid receptor **(d)**. Cells were treated with increasing concentrations of dexamethasone or dihydrotestosterone (DHT) for 1h prior to cell lysis and LUMIER assay. Relative HSPA8 interaction values (no inhibitor = 1) were fitted to a three-parameter dissociation curve with Graphpad Prism. Error bars indicate standard deviation.

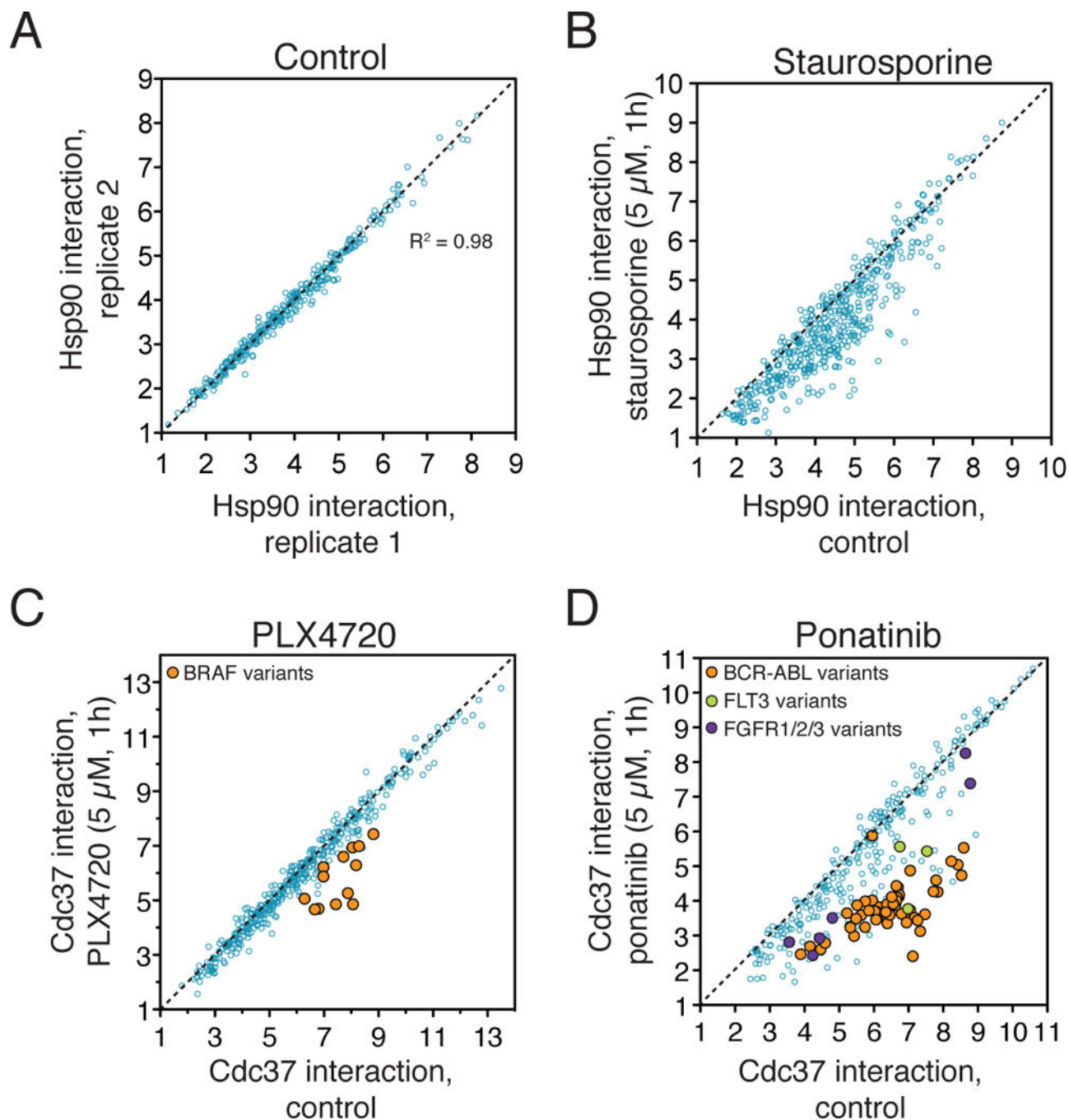


Figure 5. Profiling kinase inhibitor specificities with the chaperone interaction assay
(a) 3xFLAG-tagged kinase collection (blue circles) was transfected in duplicate into 293T cells stably expressing the *Renilla*-Hsp90 fusion protein. Two days later, kinase–Hsp90 interactions were measured with LUMIER with BACON assay. Kinase–Hsp90 interaction strength is calculated as $\log_2[\text{Hsp90}/\text{kinase}]$.
(b) The nonspecific kinase inhibitor staurosporine affects a large fraction of kinase–Hsp90 interactions. Kinases were transfected in quadruplicate into *Renilla*-Hsp90 cells. Two of the

replicates were treated with 5 μ M staurosporine and two with DMSO for 1h prior to lysis and LUMIER with BACON assay.

(c) PLX4720 is a specific BRAF inhibitor. 293T cells stably expressing CDC37-*Renilla* luciferase fusion protein and transfected with 3xFLAG tagged kinases were treated with PLX4720 (5 μ M, 1h) or vehicle prior to the assay. PLX4720 specifically affects the interactions between BRAF variants (orange circles) and CDC37.

(d) Ponatinib targets multiple kinases. The experiment was performed as in **(c)**, except that cells were treated with 5 μ M ponatinib for 1 hour prior to cell lysis and LUMIER with BACON assay. The known targets of ponatinib, ABL1, FLT3 and FGFR family receptors are indicated as orange, green and purple circles, respectively.

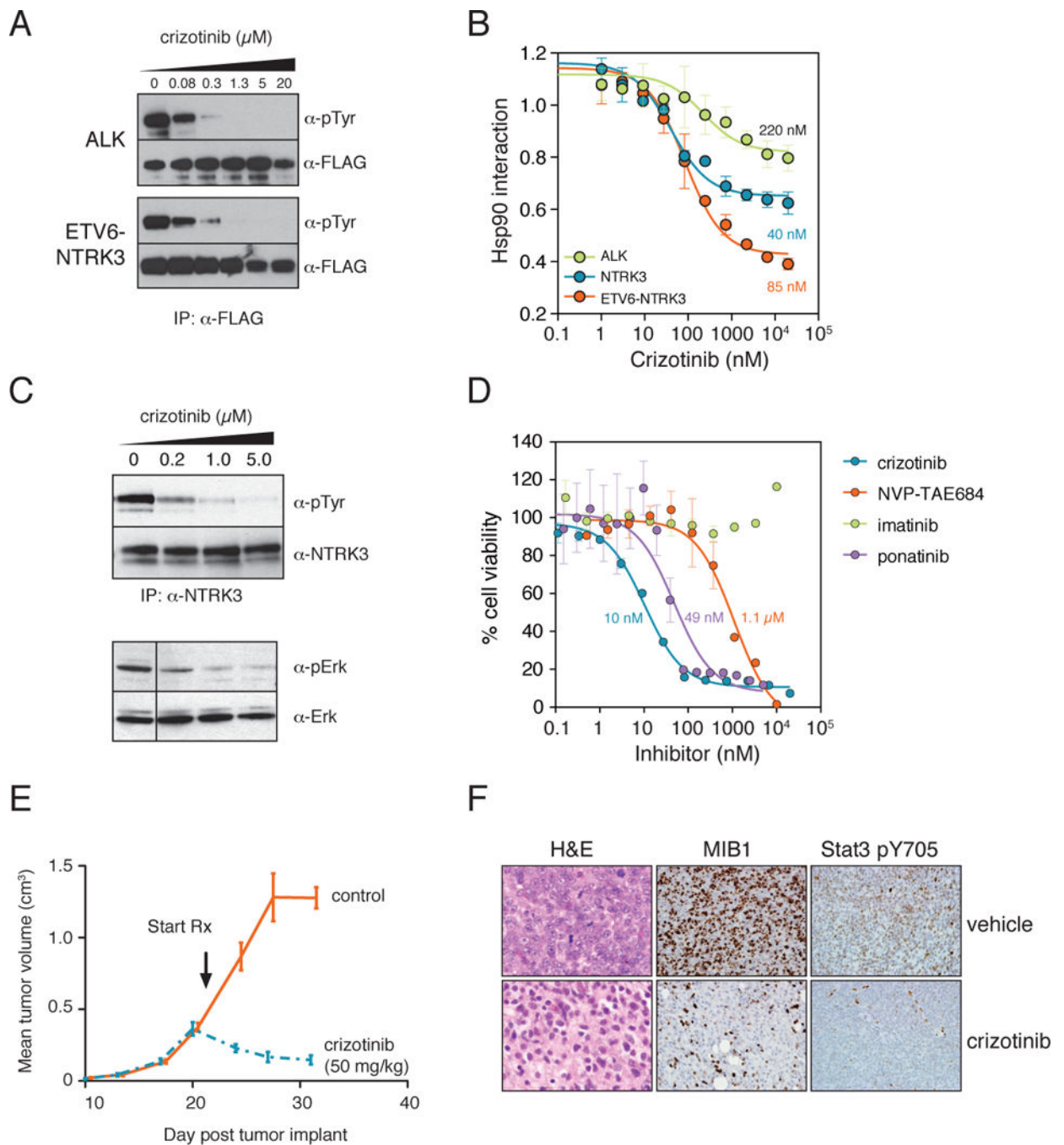


Figure 6. Crizotinib inhibits the ETV6-NTRK3 translocation fusion kinase

(a) 3xFLAG tagged ALK and ETV6-NTRK3 were transfected into 293T cells. Cells were treated with indicated concentrations of crizotinib for 1h prior to cell lysis and immunoprecipitation with anti-FLAG antibody. Kinase autophosphorylation was assessed with anti-phosphotyrosine antibody, and the efficiency of immunoprecipitation was measured with an anti-FLAG antibody.

(b) Crizotinib potently disrupts the ETV6-NTRK3–HSP90 interaction. Indicated 3xFLAG tagged kinases were transfected into *Renilla*-Hsp90 cells and the cells were treated with

increasing concentrations of crizotinib for 1h prior to cell lysis and the LUMIER assay. Relative Hsp90 interaction values (no inhibitor = 1) were fitted to a three-parameter dissociation curve with Graphpad Prism. Error bars indicate standard deviation.

(c) Crizotinib treatment leads to decreased ETV6-NTRK3 phosphorylation and downregulation of downstream MAPK-ERK signaling. MO91 cells were treated with indicated concentrations of crizotinib for 1h. After cell lysis, ETV6-NTRK3 was immunoprecipitated from the lysate with an anti-NTRK3 antibody and kinase autophosphorylation status was assessed with a phosphotyrosine-specific antibody. The activity MAPK-ERK signaling, downstream of NTRK3, was tested with a phospho-Erk antibody.

(d) MO91 cells are exceedingly sensitive to crizotinib. MO91 cells were treated with increasing concentrations of the ALK inhibitors crizotinib and NVP-TAE684 or with the ABL1 inhibitors imatinib and ponatinib or 48 hours. Cell viability was measured with alamarBlue assay. Error bars indicate standard deviation.

(e) Regression of MO91-TA xenografts upon crizotinib treatment. Sixteen nude mice were subcutaneously injected with 5×10^6 MO91-TA cells each. When the tumor size reached $\sim 350 \text{ mm}^3$, eight mice were treated with 50 mg/kg crizotinib and eight with vehicle only, using a gavage needle. Tumor size was measured with a caliper.

(f) Immunohistochemical analysis of crizotinib-treated tumor xenografts. Crizotinib-treated tumors and control tumors were surgically removed from mice and stained with hematoxylin and eosin (left panel) or immunohistochemically stained for proliferation marker MIB1 (middle panel) or for Stat3 phosphorylation at tyrosine 705 (right panel).